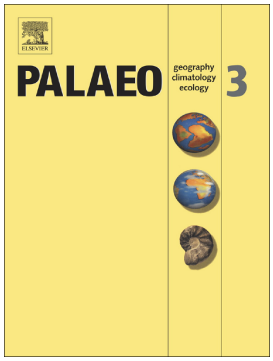

Investigating the duration and termination of the Early Paleozoic Moyero reversed polarity Superchron: Middle Ordovician paleomagnetism from Estonia

J. Michael Grappone, Thom Chaffee, Yukio Isozaki, Heikki Bauert, Joseph L. Kirschvink

PII: S0031-0182(17)30206-7
DOI: doi: 10.1016/j.palaeo.2017.07.024
Reference: PALAEO 8375

To appear in: *Palaeogeography, Palaeoclimatology, Palaeoecology*

Received date: 22 March 2017
Revised date: 23 July 2017
Accepted date: 24 July 2017

Please cite this article as: J. Michael Grappone, Thom Chaffee, Yukio Isozaki, Heikki Bauert, Joseph L. Kirschvink , Investigating the duration and termination of the Early Paleozoic Moyero reversed polarity Superchron: Middle Ordovician paleomagnetism from Estonia, *Palaeogeography, Palaeoclimatology, Palaeoecology* (2017), doi: 10.1016/j.palaeo.2017.07.024

Investigating the duration and termination of the Early Paleozoic Moyero Reversed Polarity Superchron: Middle Ordovician paleomagnetism from Estonia

J. Michael Grappone[a,1,*], Thom Chaffee[a], Yukio Isozaki[b], Heikki Bauert[c], and Joseph L. Kirschvink[a,d],

a *Division of Geological & Planetary Sciences, California Institute of Technology 170-25, Pasadena, CA 91125, USA*
b *Dept. Earth Sci. Astron., Univ. Tokyo, Meguro, Tokyo 153-8902, Japan*
c *Institute of Geology, Tallinn University of Technology, 19086 Tallinn, Estonia*
d *Earth-Life Science Institute, Tokyo Institute of Technology, Meguro, Tokyo, 152-8902, Japan*

1 Now at Geomagnetism Laboratory, School of Environmental Sciences, University of Liverpool, Liverpool L69 7ZE, UK
* Corresponding Author. Email address jmgrappone@gmail.com (J. M. Grappone)

1. Introduction

Ever since their discovery nearly 50 years ago, geomagnetic superchrons have been a puzzle for the geophysical community. Although there have only been a few during Phanerozoic time, Driscoll and Evans (2016) recently proposed multiple superchrons during the Proterozoic. Biggin et al. (2012) suggested that superchrons are the result of low heat flow at the Core Mantle Boundary (CMB), which causes low dynamo activity, and that they are generally separated by 180-190 Myr. According to Courtillot and Olson (2007), one potential process for ending a superchron is via the generation of a superplume at the bottom of the mantle, followed by the eruption of a large igneous province (LIP) 10-20 Myr later. However, this theory is unable to explain the Middle Cretaceous LIP activity and recent modelling favors a longer plume rise-time of 20-50 Myr (Biggin et al., 2012).

The two well-studied superchrons are the Cretaceous Normal Polarity Superchron (CNPS) (Helsley and Steiner, 1969) and the Kiaman Reversed Polarity Superchron (KRPS) (Irving and Parry, 1963; Kirschvink et al., 2015; McMahon and Strangway, 1968), both of which were followed a few million years later by LIPs. A third Phanerozoic superchron, during the Ordovician, was proposed as a consequence of the polarity bias study conducted in Algeo (1996). Gallet and Pavlov (1996) sampled the Moyero River section in northwestern Siberia and found further magnetostratigraphic evidence for a superchron, with a possible link to the end-Ordovician mass extinction event. They demonstrated a long period of reversed polarity from the Lower Ordovician through to the Middle Ordovician, covering the entire 15 Myr Arenig Siberian stage. Pavlov and Gallet (1998) confirmed the absence of reversals during the Llanvirn. The length has subsequently been revised upward to ~20 Myr (Pavlov and Gallet, 2005; Pavlov et al., 2012). Of the Phanerozoic superchrons, the Moyero Reversed Polarity Superchron (MRPS) is the least-well understood and demands further study.

The type locality of the MRPS is the Moyero River region in Siberia, where epicontinental sedimentary rocks of the early Paleozoic occur. With regards to the Ordovician stratigraphy in that area, sedimentary gaps cannot be excluded and the Ordovician/Silurian boundary is in hiatus as well (Gallet and Pavlov, 1996). The precise duration of this superchron has not yet been calibrated by conodont biostratigraphy that, with graptolites, form the bases of intercontinental correlation for Ordovician time.

Paleomagnetics studies of Fennoscandian Ordovician limestone have been of interest for nearly 40 years. Claesson (1978) first found a stable bulk magnetization (pole position: Lat = 30°N, Long = 46°E, α_{95} = 2.2°) in Swedish limestone, with evidence of secondary components complications. Khramov and Iosifidi (2009) found a similar pole position (Lat = 18°N, Long =55°E, dp/dm = 5°/7°), in exposed lower Ordovician limestones along the Narva River, which flows into the Baltic Sea.

Several studies in the last decade in Estonia in the Lower and Middle Ordovician have consistently found reverse polarity components and poles (e.g. Preeden et al. (2008), Plado et al. (2010), and Plado et al. (2016b)). Plado et al. (2010) studied Lower to Middle Ordovician strata in Estonia and found a reverse polarity primary component (pole position: Lat = 11.4°N, Long = 39.1°E, α_{95} = 6.7°), which confirmed the Baltic plate's southern hemisphere location during the proposed time of the MRPS. These studies only show evidence of normal polarity in a high-temperature secondary component, of apparent younger age. Further study in this area is necessary to determine if a normal polarity synsedimentary magnetozone was recorded in the local stratigraphy. Our goal is to find this magnetozone and determine if the normal period that ended the MRPS exists in Estonian stratigraphy, which contains numerous conodont and graptolite zones for global correlation (Fig. 1) We further aim to determine if the normal period is short, as reported in Pavlov and Gallet (1998), or of comparable length, as reported in Algeo (1996). Previous studies suggest that a normal polarity magnetozone

should be present near the border between the *Pygodus anserinus* and *Pygodus serra* Zones and a reverse magnetozone in all the others.

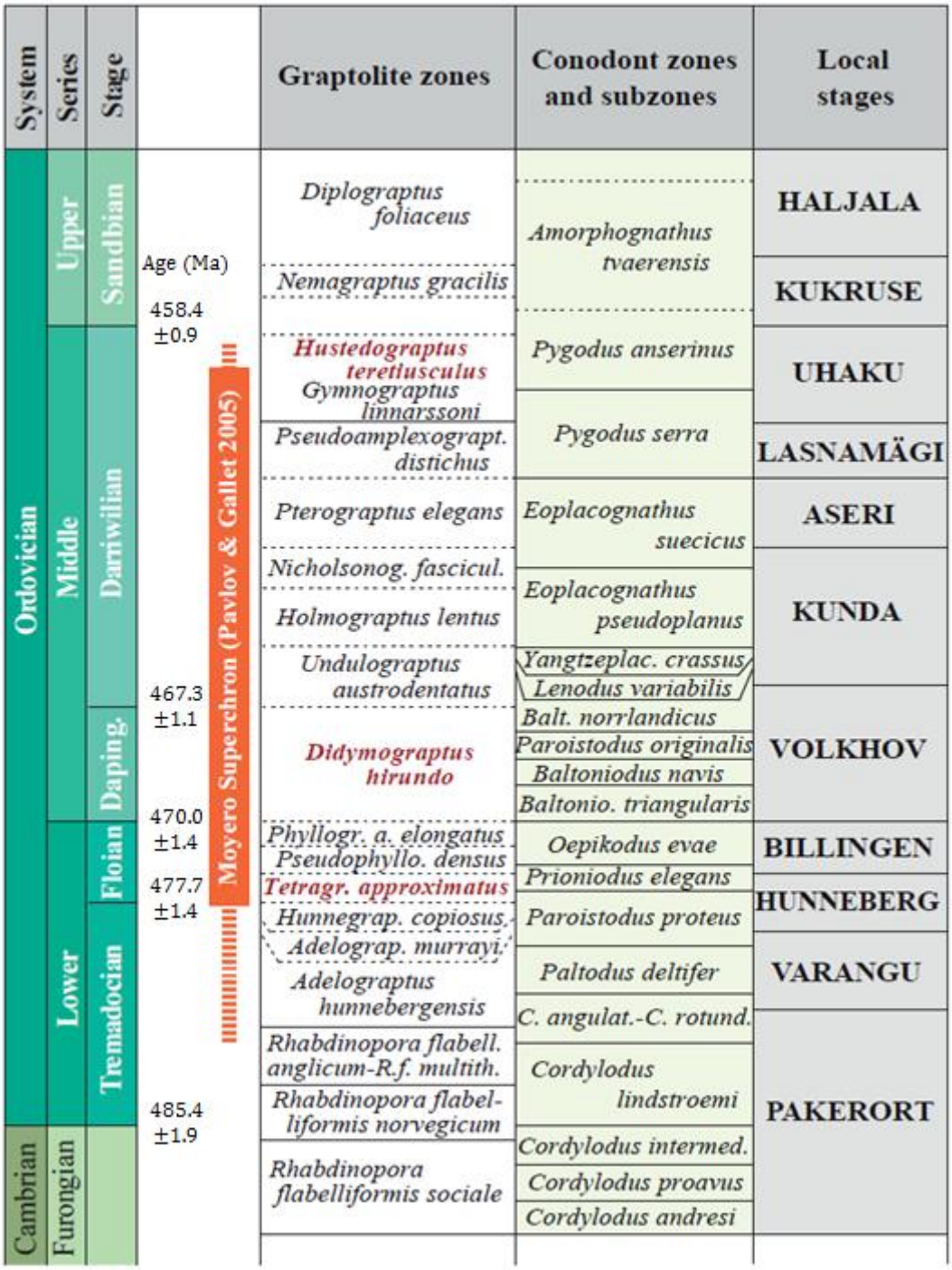

Figure 1. Geologic timescale with stages local to northern Estonia (after Meidla et al., 2014), showing the location of exposed sediment and the MRPS against the graptolite biostratigraphy in Siberia and Estonia. Ages given by Gradstein and Ogg (2012).

The Ordovician strata exposed around the Gulf of Finland are minimally tectonized, which makes the area easier to sample and simpler to study the full stratigraphy of Middle

Ordovician time and better resolve the known temporal boundaries of the superchron (Plado et al., 2010; Smethurst et al., 1998). In terms of paleomagnetics, however, the site is non-ideal. Previous studies of these rocks showed that they generally had very low magnetic moments and contained multiple magnetic minerals (maghemite, magnetite, and hematite), which made the demagnetization analysis more complex (Mertanen, 2006; Preeden et al., 2009). However, new technological developments have allowed measurement sensitivity to approach the machine noise of the SQUID magnetometer system (Kirschvink et al., 2015). When coupled with proper specimen handling to reduce magnetic noise from drilling and handling in lab, we can measure paleomagnetism from specimens too weak to be accurately measured previously, and gain extensive insight into the history of the magnetic field throughout Earth's history. The end of the MRPS by Gallet and Pavlov (1996), is a brief short normal period, which necessitated sampling intervals of 2-5 cm in order to detect it.

2. Geological setting

2.1 Tectono-sedimentary background

Estonia is located in the central part of the Baltica paleocontinent, which encompasses a major portion of northern Europe. Flat-lying terrigenous and carbonate sedimentary rocks, ranging from Ediacaran to Devonian age, cover the Archean-Proterozoic crystalline basement of the Baltic platform. These carbonate and fine siliciclastic sediments accumulated in the northern part of the Paleo-Baltic basin, which extends from Norway to the Ural Mountains in the East and from the Finnish lowland to the Trans-European (Tornquist) Suture Zone in the South. Recent studies on detrital zircons from local sandstones clarified that the main provenance of terrigenous clastics is located in the East and the South (Isozaki et al., 2014; Poldvere et al., 2014). By the end of the Ordovician, the Baltica paleocontinent had amalgamated with Avalonia and merged with Laurentia in the middle Silurian. The collision

of Baltica and Laurentia led to the Caledonian orogeny in the western periphery of Paleo-Baltic basin, but only had a negligible tectonic influence on the Estonian area.

Both the Cambrian and Devonian siliciclastic rocks as well as Ordovician–Silurian carbonate rocks are unmetamorphosed and undeformed, as they have never been deeply buried or tectonized. The Ordovician succession of mostly carbonate rocks outcrops only in northern Estonia with particular exposures along highly-weathered sheer seacoast cliffs (known as the Baltic Klint) as well as in several inland quarries, containing significantly less weathered rocks. The bedrock dips only 8'–15' (0.13°–0.25°) to the South throughout Estonia, excluding small-scale local deformations (Preeden et al., 2008). The horizontal bedding precludes the use of the usual paleomagnetic tilt test to deduce the timing of magnetic overprints (Enkin, 2003).

2.2 Middle Ordovician stages studied

Estonia's Ordovician sequence is mostly complete and has a thickness ranging from 70 to 180 m (Meidla et al., 2014). The Middle Ordovician is composed of several sedimentary units described as local stages: Volkov, Kunda, Aseri, Lasnamägi, and Uhaku in ascending order (Bauert et al., 2014; Plado et al., 2010; Smethurst et al., 1998). In northwestern Estonia, the Kunda stage records a meteoritic shower event on the Island of Osmussaar (Alwmark et al., 2010).

The base of the MRPS is rather loosely constrained to start during Tremodocian time (Lower Ordovician) (Fig. 5 in Pavlov and Gallet, 2005). The superchron continued to the late Darriwilian, terminating near the *Hustedograptus teretiusculus* graptolite Zone, during the Middle Llandeilo (Pavlov and Gallet, 1998). According to Hounslow (2016), the end of the superchron appeared to have been followed by an initial fast restart of reversal rates. A stratigraphic framework coupled with magnetic susceptibilities was put together by Plado et

al. (2016a), through surveys of the Pakri Penninsula (Middle Ordovician: upper Dapingian-upper Darrwilian). Limestone is the predominant lithology from the localities investigated, but it varies in composition depending on the stage. According to Meidla et al. (2014), the Ordovician limestones formed from cold-water carbonates, which were deposited in a shallow marine basin. Initially, the basins were rather sediment-starved, but the sedimentation rates increase upwards through the Ordovician succession.

The Volkhov stage is the oldest studied unit and straddles the Dapingian-Darriwilian boundary (Plado et al., 2010). This stage consists of glauconitic limestone, which has undergone partial to full dolomitization (Hints et al., 2012). The Kunda stage in northwestern Estonia consists of sandy limestone with kerogene and dolostone inclusions (Hints, 2014; Hints et al., 2012). The Aseri stage in northern Estonia consists primarily of biomicritic limestone, containing fine grain particles with abundant ferriferous ooids (Bauert et al., 2014; Hints, 2014). The overlying Lasnamägi Stage is characterized by slightly argillaceous biomicritic limestones which are occasionally dolomitized. Uhaku is the youngest stage studied, and its lower part in the study area is composed of very fine-grained, clay-poor limestone while moderately to highly argillaceous limestone prevails in the upper part (Bauert et al., 2014; Plado et al., 2010).

2.3 Biostratigraphy

Conodonts are the best biostratigraphic markers for the Middle Ordovician of the Baltic Platform (Fig. 1), though the limestone in the area of the Gulf of Finland is rich in trilobites, cephalopods, and other fossils as well (Smethurst et al., 1998). According to Hints et al. (2012), the conodonts are well-preserved, giving a temporal resolution of 0.1 Myr, and the low Conodont Alteration Index (CAI ~1) (Epstein et al., 1977) implies burial temperatures were significantly less than 100°C. The low CAI suggests that Lower Paleozoic

rocks in Estonia were never deeply buried during Phanerozoic time. Limestone sedimentation rates, calibrated via the conodont and chitinozoan biostratigraphy, increase upwards and imply an increasing rate of carbonate production (Meidla et al., 2014). Our sampling runs from the *Baltoniodus triangularis* Zone up into the *Pygodus anserinus* Zone.

3. Sites and samples

We studied 4 sites: the Väo limestone quarry in the eastern suburb of Tallinn, the Kunda-Aru limestone quarry near the town of Kunda in northern Estonia, cliffs near the Saka settlement in NE Estonia, and a similar succession of Ordovician rocks at the Uuga cliff on the Pakri Cape in NW Estonia (Fig. 2).

From these sites, 437 cylindrical cores (2.5 cm diameter) were drilled using portable gasoline-powered, non-magnetic, diamond-tipped drills, as detailed in Table 1. Samples were oriented using standard magnetic and solar compass techniques. Most days on the Baltic Sea were cloudy, so the majority of samples lacked solar compass measurements.

Table 1.
Sample collection by site and local stage. The superchron starts below the Volkhov stage and terminates in the Uhaku stage

Site	Volkhov Samples (coverage in cm)	Kunda Samples (coverage in cm)	Aseri Samples (coverage in cm)	Lasnamägi Samples (coverage in cm)	Uhaku Samples (coverage in cm)
Väo quarry	--	15 (70)	11 (47)	102 (371)	89 (1085)
Uuga cliff	27 (133)	--	1 (4)	43 (250)	31 (300)
Kunda-Aru quarry	--	15 (83)	16 (101)	28 (250)	--
Saka cliff	37 (236)	15 (116)	--	--	--

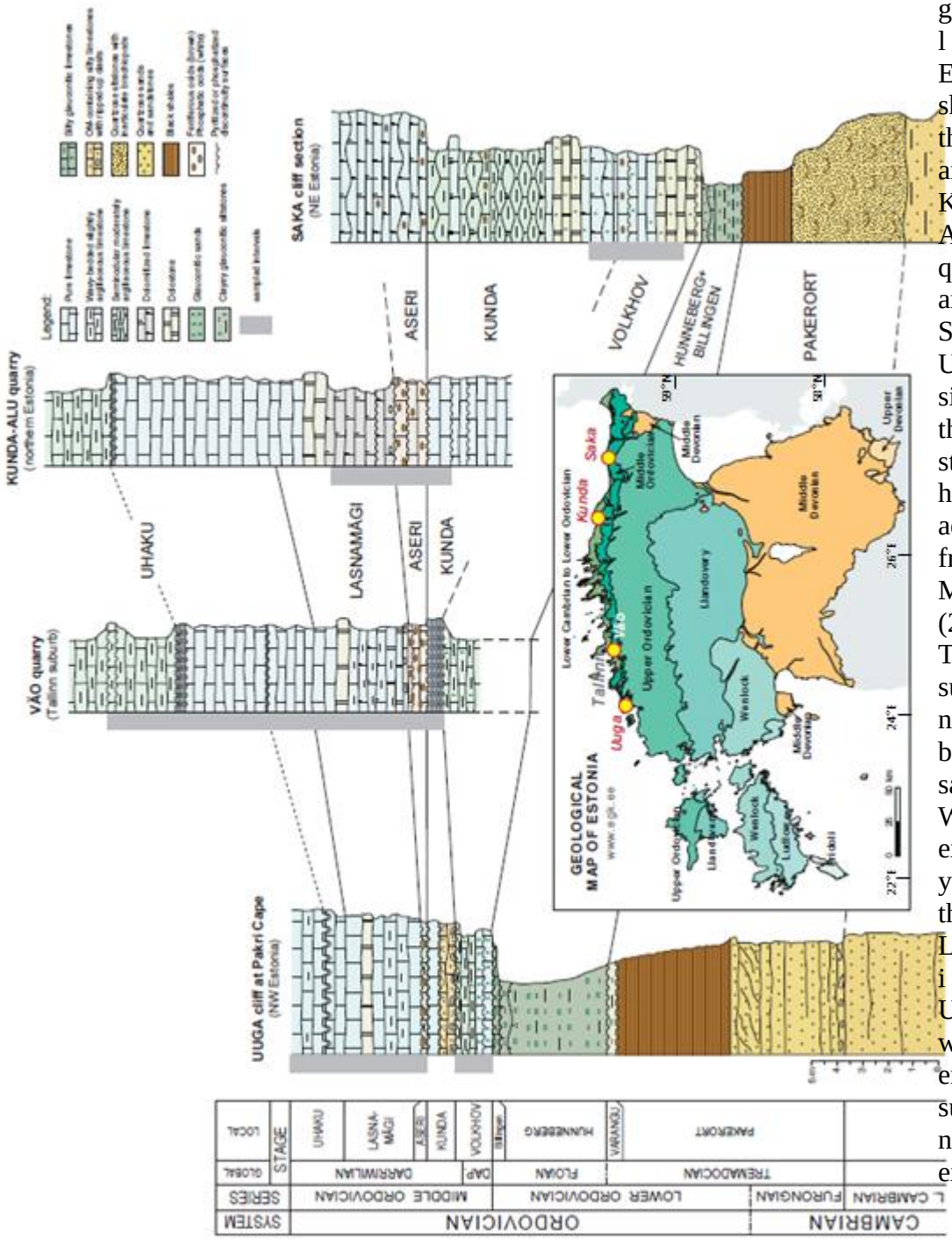

Figure 2. A generalized geological map of Estonia, showing the Väo and Kunda-Aru quarries, and the Saka and Uuga sites and their stratigraphy adapted from Meidla (2014). The superchron begins below our sampling. We most extensively covered the Lasnamägi and the Uhaku, where the end of the superchron is expected.

4. Materials and methods

For this study, we followed the procedures outlined in Kirschvink et al. (2015) and Kirschvink et al. (2008) with special attention to minimizing magnetic noise caused by stray ferromagnetic materials introduced during laboratory handling. The low volume-normalized magnetic moments reported by Plado et al. (2010) and Preeden (2009) and the small number of samples expected to display a characteristic component gained during brief normal period (Pavlov and Gallet, 1998) mandated additional care.

4.1 Sample preparation

Each core was cut into 1-cm height, 2.54 cm diameter cylindrical specimens using a three-bladed, non-magnetic diamond-impregnated rock cutting saw. Each specimen was labeled using non-magnetic, thermal-resistant ink for use in the demagnetization experiments. We washed the first useable specimen from each core in a 12 N HCl solution by submerging them for 1 second using plastic tongs and immediately rinsed them with deionized water. The acid reacted with the surface carbonates, removing metallic contaminants from the drilling and sample preparation procedures, without causing any noticeable change in the dull gray color. The specimens were then taken inside magnetically shielded (< 200 nT) rooms and kept inside for the remainder of the study. We blew all surfaces clear of dust and debris after every 3-4 demagnetization steps to mitigate any ferromagnetic aerosol contamination. We used disposable, dust-free nitrile gloves to handle the specimens during the demagnetization and measurement process.

4.2 Paleomagnetism

All remanence measurements were conducted on two superconducting rock magnetometers housed in magnetically shielded rooms at Caltech. Both magnetometers have

background instrument sensitivity of approximately $4 \times 10^{-13}\mathrm{Am}^2$ when run in a "sham mode" without the sample holder. We used 19 mm diameter (1 mm thickness) quartz tubes that were soaked in a 12N HCl acid bath for 3 days before use. During use, we subjected the empty holders to maximum strength alternating-field (AF) demagnetization after every 9th specimen. The magnetic moment increased to an average of approximately $2.2 \times 10^{-12}\mathrm{Am}^2$ with the holder installed, with a minimum approaching the machine's resolution.

We employed a hybrid demagnetization strategy which has proven effective in the separation of magnetic components on drab-colored, weakly magnetized specimens in previous studies (e.g. Ward et al. (1997)). We measured the natural remanent magnetization (NRM) for each specimen. We then cooled the specimens in liquid nitrogen baths for at least 30 minutes to remove viscous components potentially carried by muti-domain (MD) magnetite grains by cycling them through the Verway transition (~ 120 K). We then subjected the specimens to alternating-field (AF) demagnetization at field strengths of 2.5, 5.0, and 7.5 mT to remove any soft components caused by the transportation or preparation of the specimens. We thermally demagnetized the specimens in an inert (N_2) atmosphere, magnetically-shielded oven (< 25 nT net field) in incremental temperature steps (5–30°C) from 80°C up to a maximum of 575°C. We continued the temperature steps on each specimen until its orthogonal projection diagram displayed unstable behavior in the data. We ran 408 specimens until their data became erratic, which occurred at temperatures ranging from 200°C to 575°C. We then determined principle magnetic components using the methods outlined in Kirschvink (1980) and allowed for Maximum Angular Deviations (MADs) of 15°. Similarly to Kirschvink et al. (2015), many specimens displayed a presumed characteristic component in the 300-500°C range, but their data became too unstable before reaching the origin or forming a stable endpoint cluster. We used least-squares great circle

fits anchored at the origin to extract the missing data, following the method of McFadden and McElhinny (1988).

4.3 Rock magnetism

After the initial paleomagnetic analysis, we selected 23 (10% of those showing at least one stable component) specimens as representative specimens for the rock magnetism study. The specimens were selected taking into account the sampling site, whether the specimen lost magnetic stability at a lower (≤300°C) or at a higher (≥300°C) temperature, and their local stage. Due to the low magnetic moment of the specimens, rather than using the front chip, the weathered surface, for the rockmagnetics survey, the .2 specimen in the core was used for the experiments to improve the signal-to-noise ratio. We subjected them to the same rockmagnetic experiments outlined in Kirschvink et al. (2008), including progressive AF demagnetization up to a peak field of 80 mT, followed by the anhysteric remanent magnetization (ARM) Lowrie-Fuller test for single-domain behavior (Johnson et al., 1975). The ARM was acquired progressively using peak alternating fields of 100 mT, with the DC bias ranging from 0-1 mT. The maximum ARM was then demagnetized using progressive AF. An IRM pulse in a peak field of 100 mT was then applied to the specimens, which was then followed by progressive AF demagnetization (Johnson et al., 1975). Progressive IRM acquisition experiments were then applied up to 350 mT, which were followed by progressive AF demagnetization.

5. Results

5.1 Rock magnetics

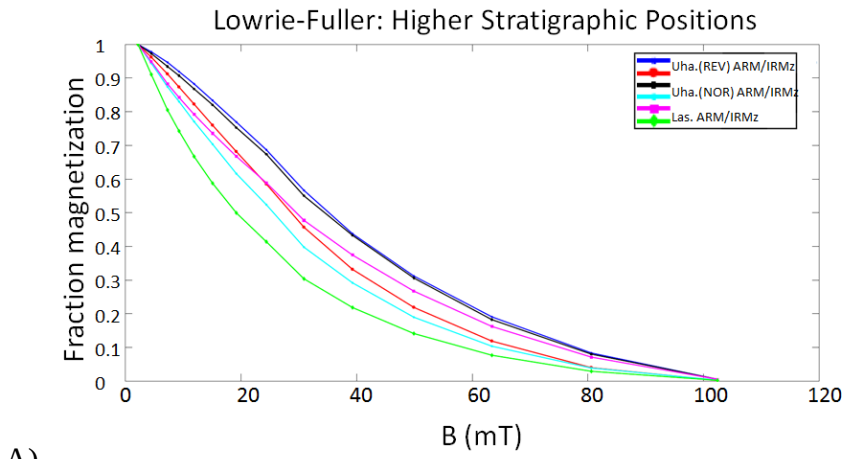

A)

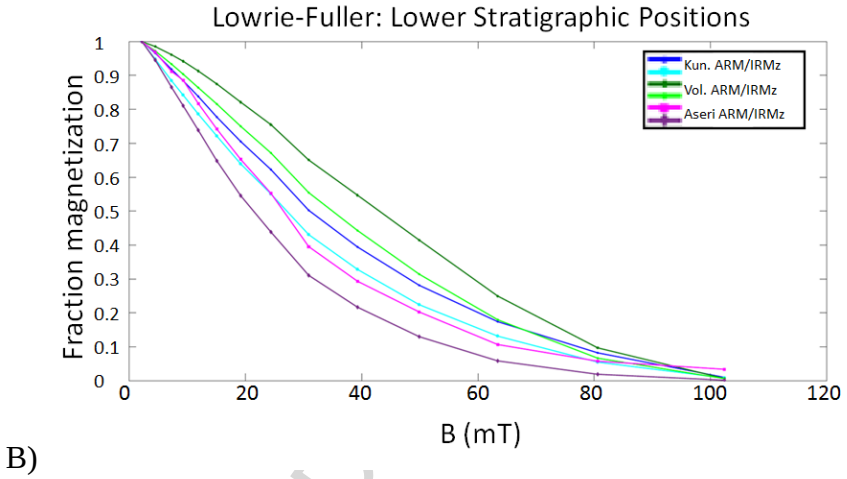

B)

Figure 3. Characteristic Lowrie-Fuller curves representative of all studied sections. All specimens have an ARM curve above the IRMz curve, which is characteristic of predominately single-domain grain mineralogy. The higher stratigraphic sections (A) are the Lasnamagi and Uhaku stages. The lower stratigraphic sections (B) are the Volkhov, Kunda, and Aseri stages.

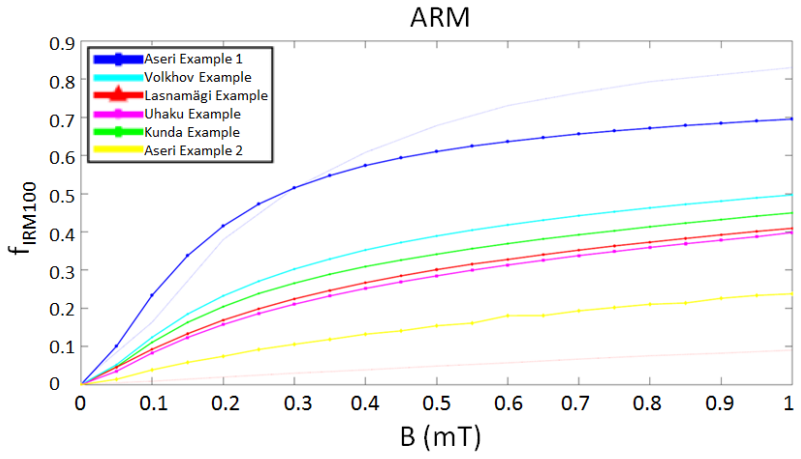

Figure 4. ARM curves selected as representative for stratigraphy. The upper reference curve is for the highly non-interacting magnetotactic bacteria and the lower reference line is for the highly interacting chiton tooth references samples after Kobayashi et al. (2006). The data indicate increasing interactivity with decreasing age, except for the Aseri samples, which show bimodal behavior, unrelated to sampling site.

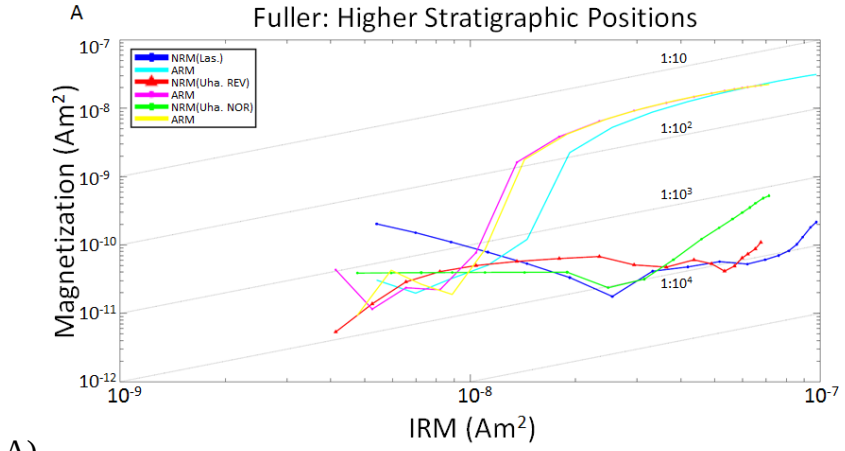

A)

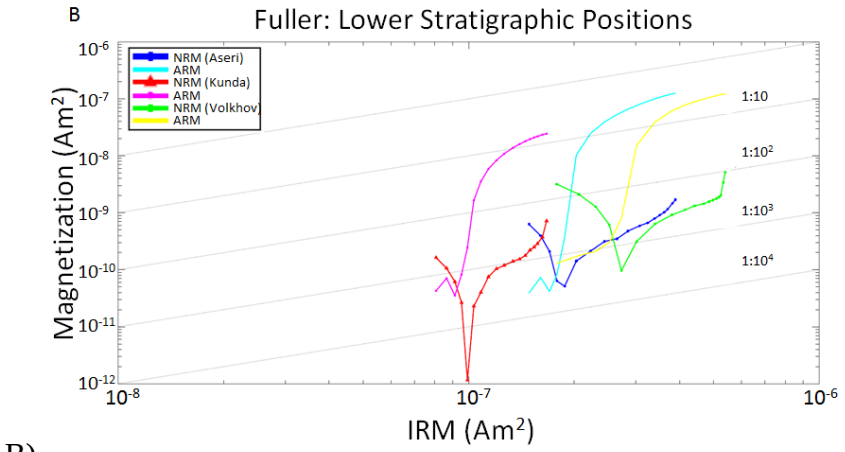

B)

Figure 5. Fuller test curves representative of the local sections. The NRM curves are over 2 orders of magnitude below the IRM and almost 2 orders of magnitude below the ARM curves. These data are characteristic of a deposition remanent magnetization. The higher stratigraphic sections (A) are the Lasnamagi and Uhaku stages. The lower stratigraphic sections (B) are the Volkhov, Kunda, and Aseri stages.

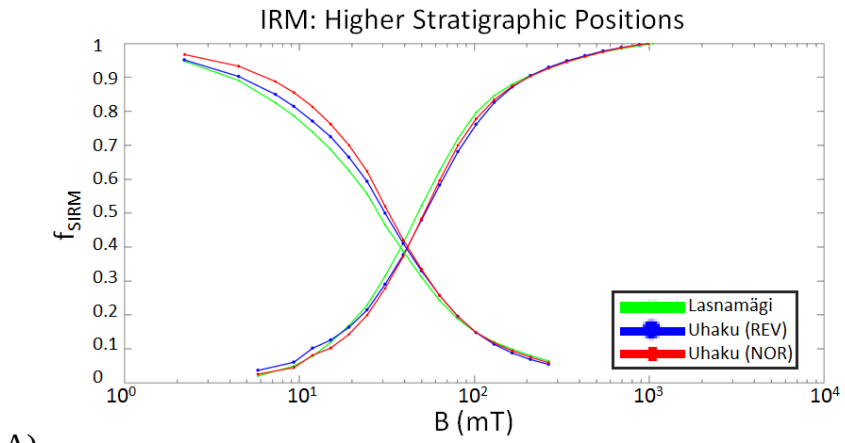

A)

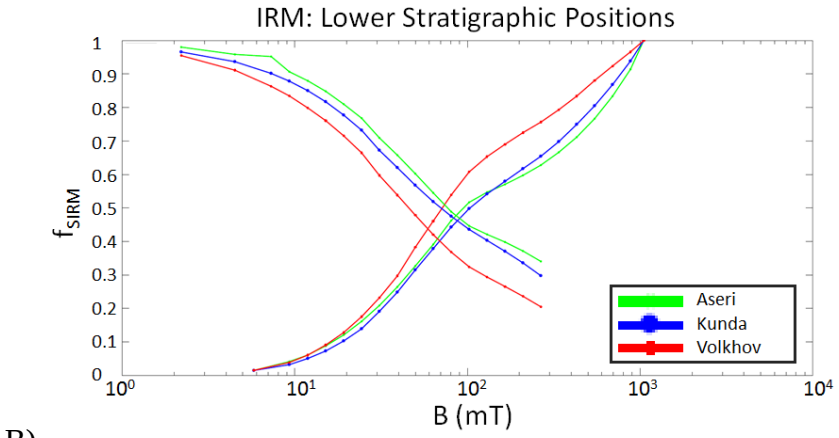

B)

Figure 6. IRM acquisition curves representative of the local sections. The curves have destructive field values ranging from 30-110 mT. Non-flattening curves are characteristic of the presence of a high coercivity mineral, like hematite. The higher stratigraphic sections (A) are the Lasnamagi and Uhaku stages. The lower stratigraphic sections (B) are the Volkhov, Kunda, and Aseri stages.

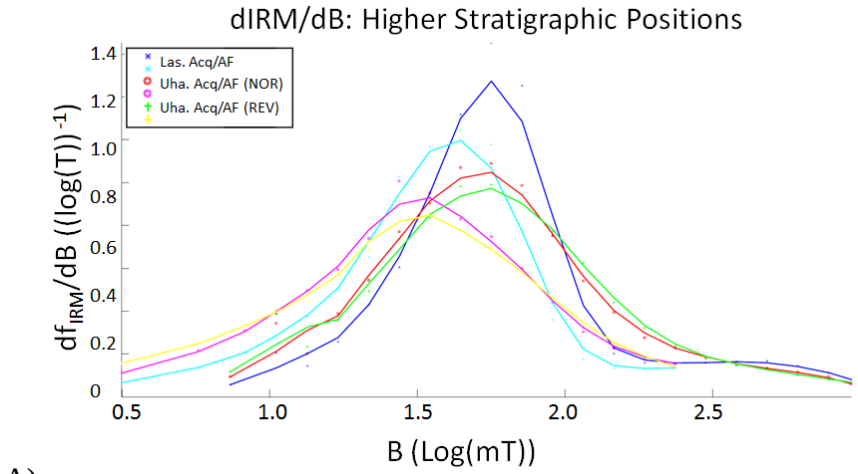

A)

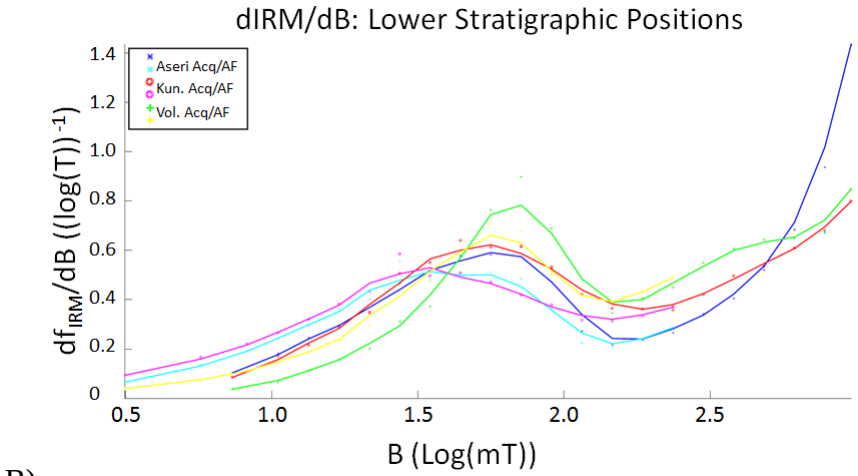

B)

Figure 7. Curves showing dIRM/dB spectra (the derivative of Figure 6) selected to represent the various specimens. These curves show more variation than other data found in the rockmagnetic study but are well-correlated with stratigraphic section. Most samples show a peak generally characteristic of magnetite and a second characteristic of a high susceptibility mineral, like hematite. The latter peak is absent in the Uhaku samples. The higher stratigraphic sections (A) are the Lasnamagi and Uhaku stages. The lower stratigraphic sections (B) are the Volkhov, Kunda, and Aseri stages.

The ARM version of the Lowrie-Fuller test (Johnson et al., 1975) (Fig. 3) indicates primarily single domain (SD) magnetic particles. For every specimen, the progressive AF demagnetization of the ARM curve remains above that of the IRM, which indicates predominately SD behavior. The spacing of the curves indicates the effects of interparticle interaction, but the apparent variation has no clear pattern.

The interparticle interaction characteristics were determined by ARM acquisition in

the coercivity band < 100 mT and show a mixture of interacting and non-interacting particles (Fig. 4). All the data plot between the chiton tooth (highly interacting) and magnetotactic bacteria (highly non-interacting) reference curves (Kobayashi et al., 2006). The curves generally approach the chiton tooth reference going up in the stratigraphic section, which indicates a decreasing proportion of interacting particles.

Fuller et al. (1988)'s test of NRM origin (Fig. 5) compares the intensity of the NRM remaining during AF demagnetization with that of the IRM. The NRM values are more than 2 orders of magnitude less than the corresponding IRM levels and almost two orders of magnitude lower than the ARM levels. These results support a depositional or post-depositional remanent magnetization (DRM or pDRM) NRM signal, instead of a chemical or thermal remanent magnetization (assuming a paleofield within an order of magnitude of the current field).

Cisowski (1981)'s IRM/ARM coercivity spectral analysis (Fig. 6) shows the most variability of the rockmagnetic data. Most samples have medium destructive field values between 30 and 60 mT, but 7 have field values between 60 and 110 mT. However, half of the samples have not reached saturation at peak pulse fields of up to 300 mT, which indicates the presence of a high-coercivity antiferromagnetic phase, potentially hematite or goethite. Samples from the Lasnamägi and Uhaku stages show more clear saturation. Figure 7 shows the derivate of the IRM acquisition curves in Figure 6. They show either one or two peaks for the samples: one around 180 mT and a second above 250 mT. The former is characteristic of magnetite, but the broad range of peak values indicates the potential for an additional moderate coercivity mineral, potentially maghemite or pyrrhotite. The latter is characteristic of hematite (Peters and Dekkers, 2003). The Lasnamägi specimens have small peaks above 250 mT, but the Uhaku specimens have no high coercivity peak, indicating low quantities of antiferromagnetic materials in these specimens.

The rockmagnetic data indicate moderately-interacting single domain grains with a DRM or pDRM dominate the specimens' mineralogy. The primary magnetic mineral indicated is magnetite, presumably of a biogenic origin, but many specimens show minimal saturation at high coercivities in Figure 6, consistent with the additional presence of hematite.

5.2 Paleomagnetics

The average NRM of the specimens was found to be very low (Table 2). After cycling in liquid nitrogen, 3-11% of the NRM intensity was lost, implying the presence of small amounts of MD magnetite undergoing a Verway transition. The quantity of MD grains in the specimens appears to be quite low, and no clear direction was obtained from the liquid nitrogen steps.

Three components were identified from orthogonal projections (examples in Fig. 8): a low-temperature component, a medium-temperature component, and a high-temperature component inferred from great circle fits. The low-temperature and medium-temperature components existed in 2 forms: convergent and non-convergent. The convergent low-temperature component has the designation P_W. Orthogonal plots displaying P_W displayed no other component. The non-convergent low-temperature component has the designation O_L. Only specimens that also had a medium-temperature component displayed O_L. The medium-temperature components (both forms) have the designation P_R or P_N, depending on polarity. The non-convergent medium-temperature components implied the potential for another, high-temperature component. Great circle fits were then used to infer the direction of the high-temperature component, O_H.

The weak NRM values meant that the specimens frequently had maximum unblocking temperatures significantly below that of the main carrier, magnetite ($585°C$). The survivorship curves in Figure 9 show that O_L generally unblocked at temperatures below

200°C and completely by 300°C. The P components had a much broader range of unblocking temperatures: 200-570°C, with 146 specimens completely unblocked by 300°C. These low-temperature specimens generally had NRM values of $2-4\times10^{-8}\ \frac{Am^2}{kg}$ and lacked a stable, convergent direction as a set. The largest drop was in the 300-400°C range, with 39% of specimens unblocking completely. Few samples remained measurable above 500°C. Table 3 shows that specimens from the quarries generally had higher maximum unblocking temperatures, which is consistent with these samples having less weathering and stronger SD magnetization (Table 2: After LN_2). No unblocking spectrum exists for O_H because no specimen had sufficient NRM remaining to characterize the component directly. Based on unblocking temperatures and convergence, 5 components were inferred from the data. Their directions are given in Table 4 and shown in Figure 10.

The components $O_L, P_R,$ and P_W all fall along a great circle with the modern field direction (within their α_{95} ellipses). Their alignment implies that the components' direction vectors are related linearly. O_H and P_N appear to be distinct from the others.

The component with the lowest unblocking temperature (up to 260°C) was P_W. It only appeared in specimens from the Pakri and Saka cliffs, which also have the most weathering. Its unblocking temperature and direction are similar to the non-convergent component, O_L (maximum unblocking temperature of 300°C), which is found in all 5 stages and 4 sites. The direction of these vectors is shown in Figure 11. The number of specimens displaying P_W is too small to use McFadden and McElhinny (1990)'s mean direction test, but the angle between the O_L and P_W vectors is 2.8°, which is less than half of the α_{95} for P_W. The difference does not appear to be sufficient to consider the difference in these directions statistically significant. The flat-lying strata preclude the use of a tilt test to determine the components' ages. Samples with maximum unblocking temperatures below 260°C were excluded from further analysis to avoid any modern field contamination in the data.

The next components resolved are the medium unblocking temperature components, P_R and P_N, for 205 samples. These components were determined using line fits on specimens with unblocking temperatures above $240°C$ with both convergent and non-convergent end points. The components generally became unstable when less than 80% of the specimen's NRM remained. All specimens from the Kunda quarry had convergent data, but many specimens from the other sites did not. All samples displaying P_N had convergent data. Figure 12 shows the P_R above ($P_{R,L\rightarrow LU}$) and below ($P_{R,UU}$) the short normal magnetozone and P_N direction data. Table 3 also includes the P_R direction extracted for the Kunda and Aseri stages, $P_{R,K+A}$, and for the Volkhov stage, the P_V. P_V is the oldest and has a statistically distinct pole (with a χ^2 p-value of 0.039 compared to $P_{R,K+A}$, the second oldest stage-level direction). No other stage-level component is statistically distinct from the others. The null hypothesis that the P_R directions does not vary by site cannot be rejected at the 95% confidence level according to McFadden and McElhinny (1990)'s mean direction test. The differences between the P_R directions by stage are relevant at the 95% confidence level, but the apparent movement of the pole has no clear direction.

The angle between the P_R and the P_N vectors is 162°, 18° off of the expected anti-pole. The large α_{95} value for P_N ($\alpha_{95} = 25.5°$) means that the anti-pole of P_R falls within the 95% confidence interval and is thus insufficient to reject the null hypothesis that they are anti-polar. The short normal magnetozone occurs 66-110 cm above the Lasnamägi/Uhaku boundary from the Uuga cliffs and 30-39 cm above the Lasnamägi/Uhaku boundary from the Väo quarry. Their direction data are plotted in Figure 13 as a function of stratigraphic position. We observe three magnetic polarity intervals: 2 reversed intervals, interrupted by a short normal polarity interval. The magnetostratigraphy plots indicate that the observed scatter does not appear to be the result of the pole's location changing during the superchron.

The final component inferred is the high-temperature component: O_H, which is shown in Figure 14. No unblocking temperature was determined for this component because the samples lacked sufficient NRM to characterize the component directly. This component was extracted using great circle fits on samples that had a non-convergent medium-temperature component. Running the category B reversals test (McFadden and McElhinny, 1990) of the O_H direction against the P direction gives a χ^2 p-value of 5.9×10^{-7}, which means the null hypothesis that the directions are antiparallel can be rejected. The direction of O_H is distinct from that of P_R and its anti-pole, which means that O_H is not a false positive from the great circle fits. The direction of O_H falls within the α_{95} uncertainty cone of P_N, but only exists in samples that display a non-convergent medium-temperature component. The direction of O_H is also distinct (χ^2 p-value $< 10^{-6}$ in a mean direction test) from the modern field.

Table 2.
Average magnetization values for specimens by site.

Site	NRM ($\frac{Am^2}{kg}$)	After LN_2 ($\frac{Am^2}{kg}$)	At last stable step ($\frac{Am^2}{kg}$)
Väo (quarry)	5.62×10^{-8}	5.10×10^{-8}	7.38×10^{-9}
Kunda (quarry)	2.89×10^{-7}	2.72×10^{-7}	1.38×10^{-8}
Saka (seaside)	7.30×10^{-8}	7.09×10^{-8}	6.17×10^{-9}
Pakri (seaside)	5.42×10^{-8}	4.81×10^{-8}	1.26×10^{-8}

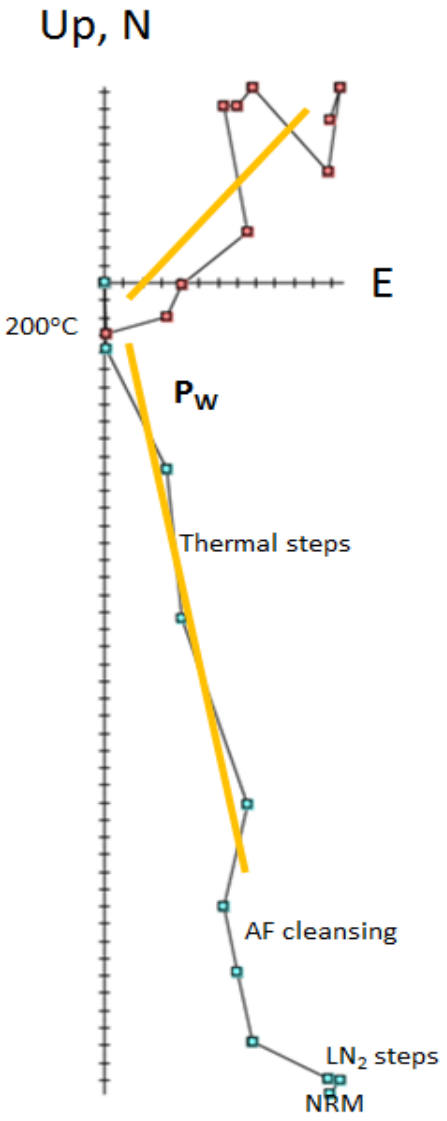

A)

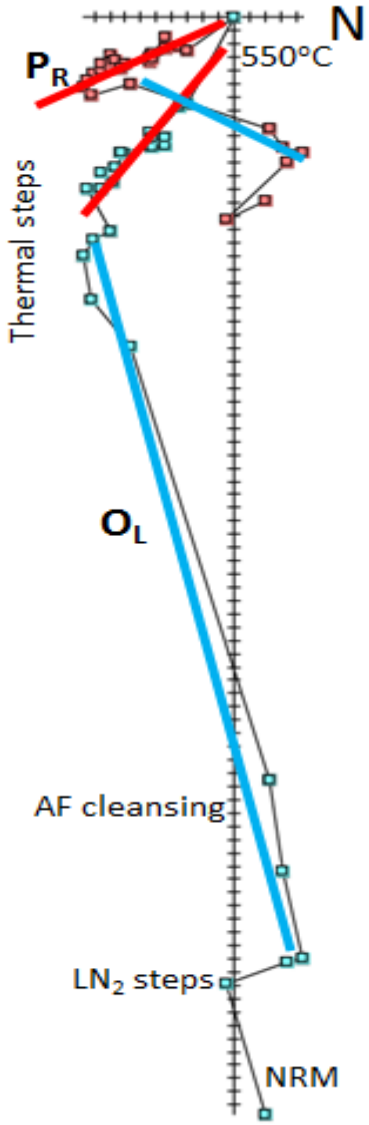

B)

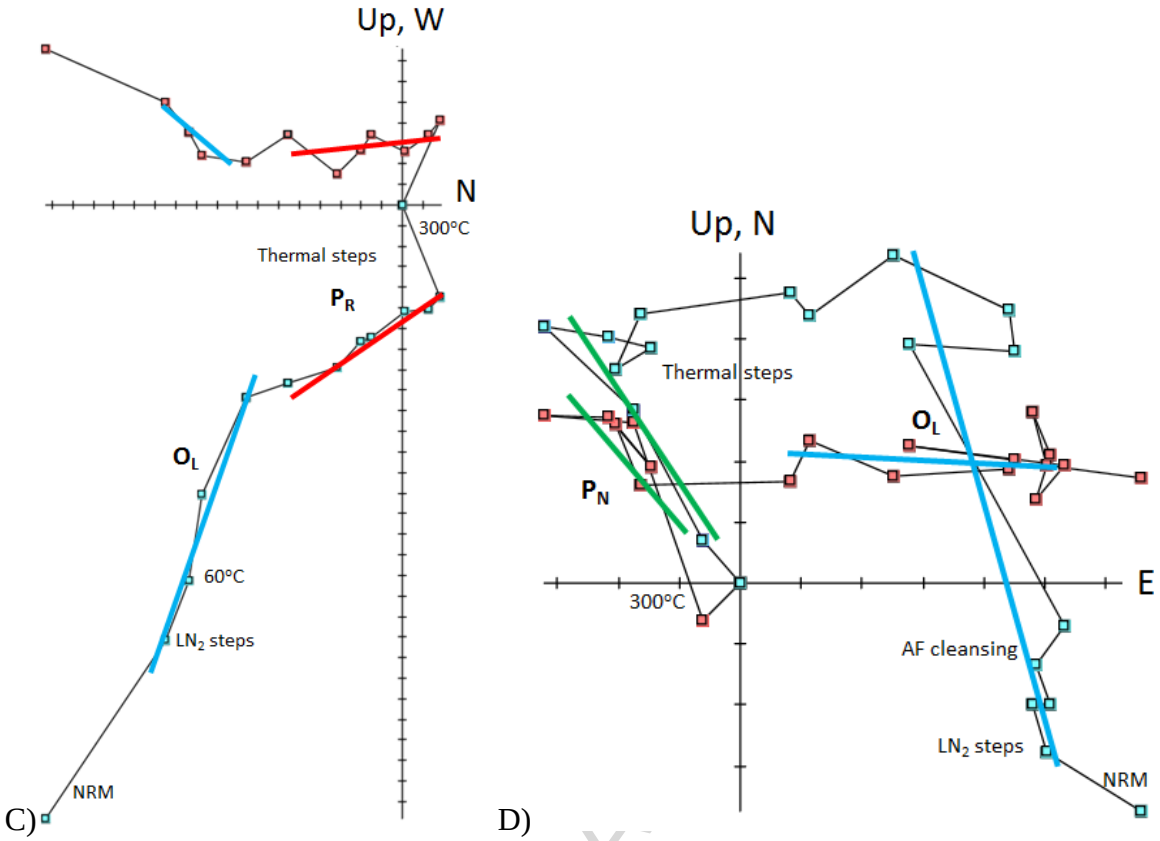

Figure 8. Examples of progressive demagnetization orthographic projections, showing the different components extracted. A) Specimen from the Saka cliffs, Volkhov stage (170 cm from base) showing the P_W singular low unblocking temperature (200°C) component that terminates at the origin. B) Specimen from the Kunda-Aru quarry, Aseri stage (75 cm from base), showing the O_L and P_R components, with one of the highest unblocking temperatures observed: 550°C. C) Specimen from the Väo quarry, Uhaku stage (655 cm from base), displaying O_L and P_R but not terminating at the origin. D) Specimen from the Pakri cliff, Uhaku stage (66 cm from base), displaying O_L and P_N.

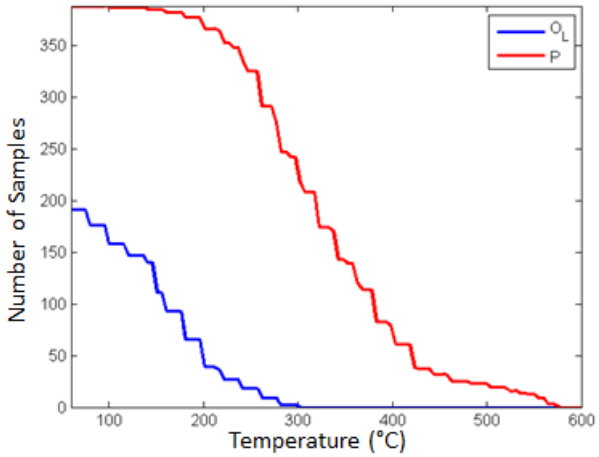

Figure 9. Survivorship curves for $\boldsymbol{O_L}$ and $\boldsymbol{P}$ components. The cumulative unblocking spectra recorded for the $\boldsymbol{O_L}$ and $\boldsymbol{P}$ components in each specimen, as a function of temperature. Despite the apparent prevalence of magnetite in the samples, 85% of samples unblocked below 400°$\boldsymbol{C}$.

Table 3.
Maximum unblocking temperatures by sampling site.

Site	100 – 240°C	245 – 300°C	305 – 400°C	405 – 500°C	500 – 570°C
Väo quarry	24 (12%)	58 (29%)	89 (44%)	28 (14%)	3 (1%)
Uuga cliff	16 (16%)	37 (37%)	37 (37%)	6 (6%)	4 (4%)
Kunda-Aru quarry	3 (5%)	14 (24%)	23 (40%)	6 (10%)	12 (21%)
Saka cliff	18 (38%)	17 (35%)	7 (15%)	5 (10%)	1 (2%)

Table 4.
Paleomagnetic results from the Estonian Middle Ordovician sampling reported in this study.

Component[i]	N	Declination (°)	Inclination (°)	κ^{ii}	R	$\alpha 95^{iii}$(°)
$P_{R,ave}$	197	168.6	57.5	9.89	174	3.4
$P_{R,V\rightarrow LU}$	153	169.8	58.7	10.1	138	3.8
$P_{R,UU}$	44	167.0	52.6	9.65	39.5	7.3
$P_{R,K+A}$	45	159.6	58.3	13.7	41.8	6.0
P_V	29	159.2	69.6	9.07	25.9	9.4
P_w	17	40.6	82.6	36.4	16.6	6.1
P_N	8	312.1	-61.6	4.79	6.54	25.5
O_L	227	62.4	82.6	12.1	208	2.9
O_H	70 (140 arcs)	331.8	-71.9	13.7	65.0	4.9

i. $P_{R,V\rightarrow LU}$ and $P_{R,UU}$ are the medium=temperature components from the Volkhov to the lower Uhaku (during the superchron) and during the Upper Uhaku (after the short normal period) in the stratigraphy, respectively. $P_{R,ave}$ is the average of the two. $P_{R,K+A}$ is during the Kunda and Aseri stages. P_N is during the short normal period. P_w is the low unblocking temperature convergent component present in highly weathered specimens. O_L and O_H are the low- and high-temperature overprints, respectively, showing normal polarity.
ii. κ = Precision parameter (Fisher, 1953).
iii. α_{95} = 95% confidence cone.

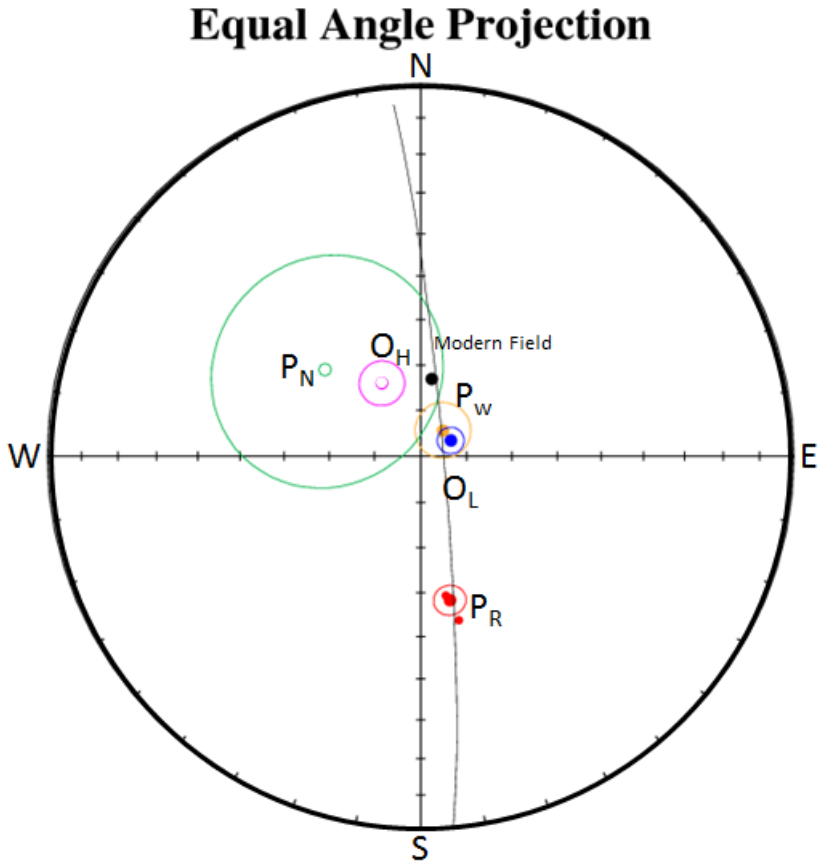

Figure 10. Equal angle projection showing the modern field and all measured directions with $\boldsymbol{\alpha_{95}}$ error ellipses. The characteristic components, $\boldsymbol{P_W}$, $\boldsymbol{P_R}$ (average, lower stratigraphically, and higher stratigraphically), and $\boldsymbol{P_N}$ are displayed along with the overprints, $\boldsymbol{O_H}$ and $\boldsymbol{O_L}$, as well as the modern field. $\boldsymbol{P_R}$, $\boldsymbol{P_W}$ $\boldsymbol{O_L}$, and the modern field direction all plot along the same circle and are likely related.

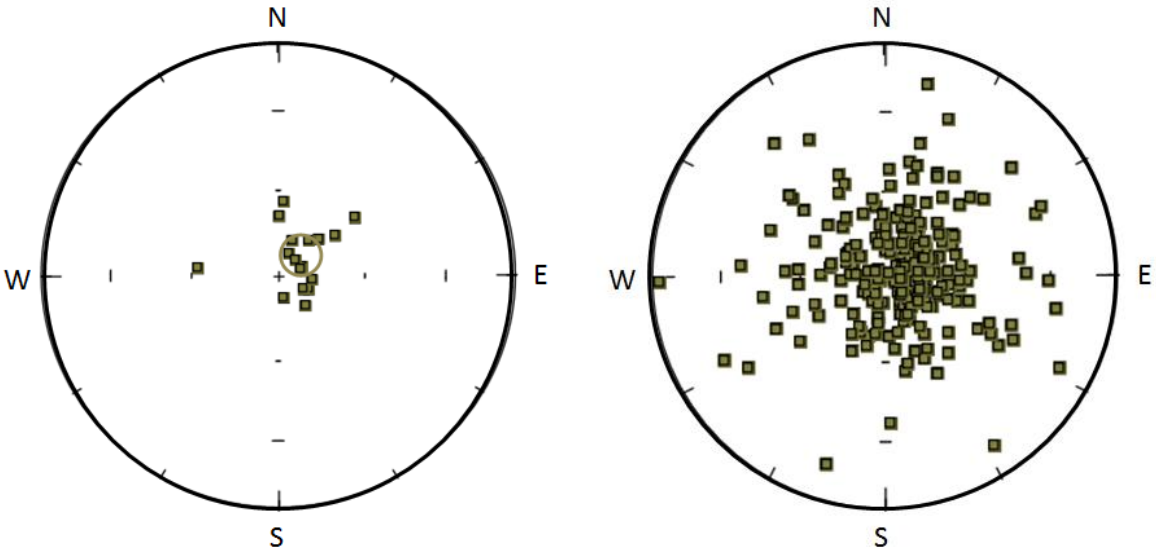

Figure 11. The direction of low unblocking temperature components. Left: the convergent component $\boldsymbol{P_W}$ observed in Pakri and Saka cliff specimens. Right: the non-convergent component $\boldsymbol{O_L}$ observed in specimens from every site. $\boldsymbol{P_W}$ unblocks by 260°$\boldsymbol{C}$ and $\boldsymbol{O_L}$ unblocks by 300°$\boldsymbol{C}$. The directions appear similar and lie between the modern field direction and the presumed paleodirection. Brown symbols indicate lower hemisphere directions and circles indicate the $\boldsymbol{\alpha_{95}}$ error ellipse.

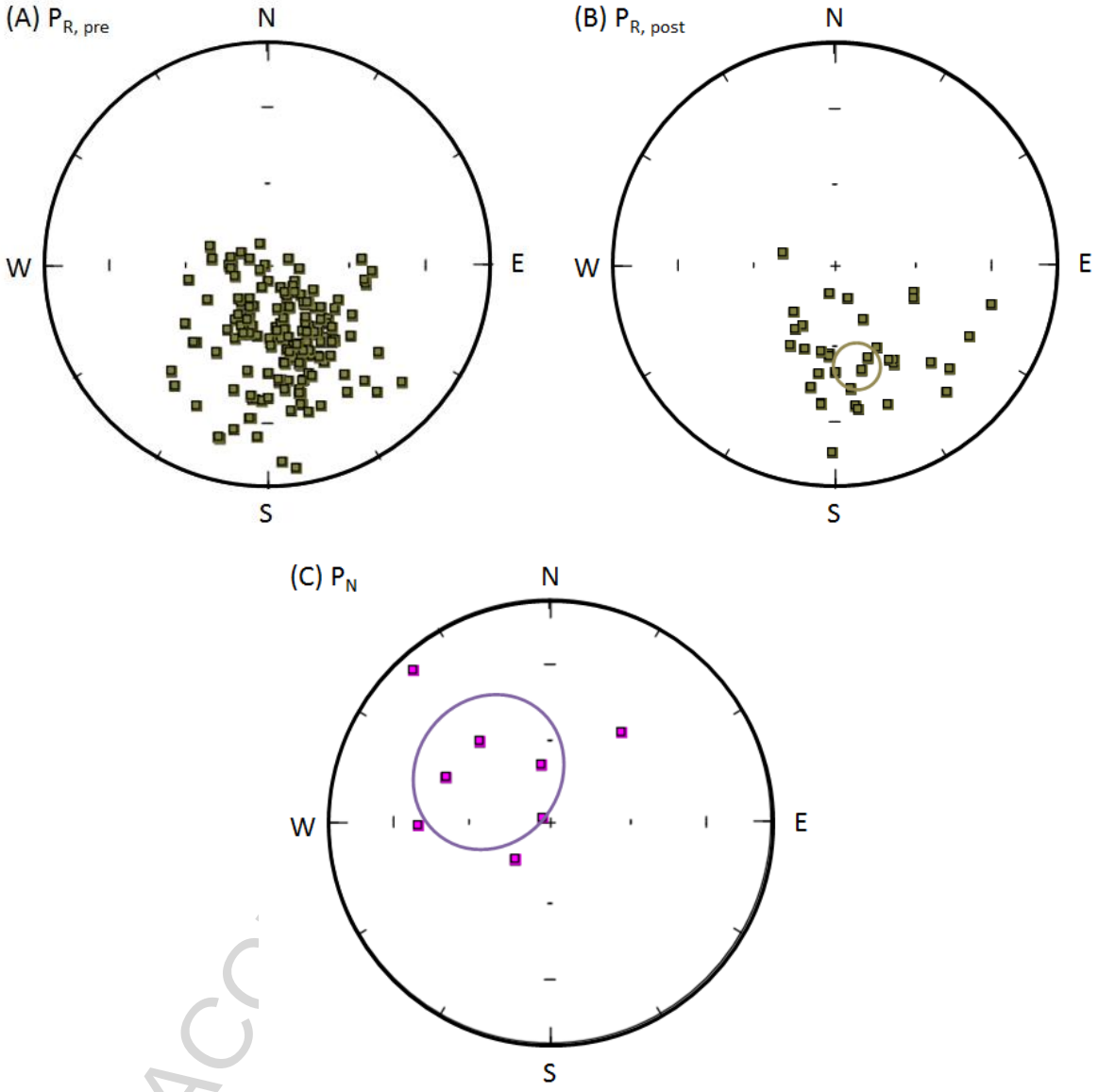

Figure 12. Equal area plot of the direction of presumed characteristic components: a) $\boldsymbol{P_{R,L\rightarrow LU}}$, b) $\boldsymbol{P_{R,UU}}$, c) $\boldsymbol{P_N}$. The $\boldsymbol{P_R}$ directions are consistent with formation in the lower hemisphere in a reversed magnetic field magnetozone, both above and below $\boldsymbol{P_N}$ in the stratigraphy. The $\boldsymbol{P_N}$ direction is sparse, with only 8 samples because the normal polarity magnetozone was short lived. Brown symbols correspond to lower hemisphere directions and purple symbols to upper hemisphere directions.

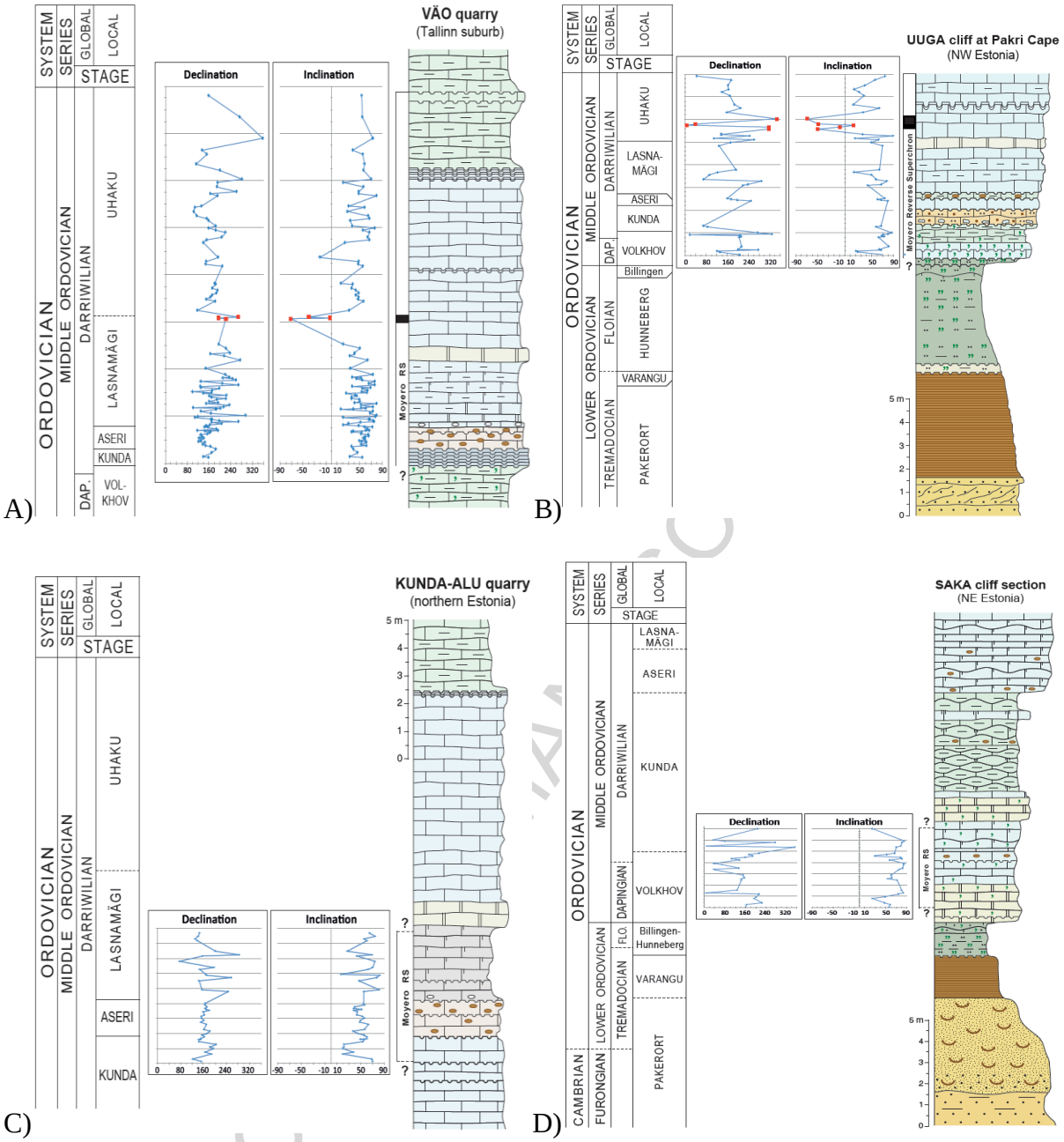

Figure 13. Magnetostratigraphy by site, based on $\boldsymbol{P_R}$ and $\boldsymbol{P_N}$. The 4 sites (A- Väo quarry, B- Uuga cliff, C- Kunda quarry, and D- Saka cliff) cover overlapping regions from the bottom of the Volkhov to the top of the Uhaku. The magnetostratigraphic data indicates the presence of the superchron in each site, which also ranges from the Volkhov to the lower Uhaku in total. The short normal period appears in both data sets that run through the Uhaku. The weak magnetization of many specimens causes a significant noise in on the specimen-level.

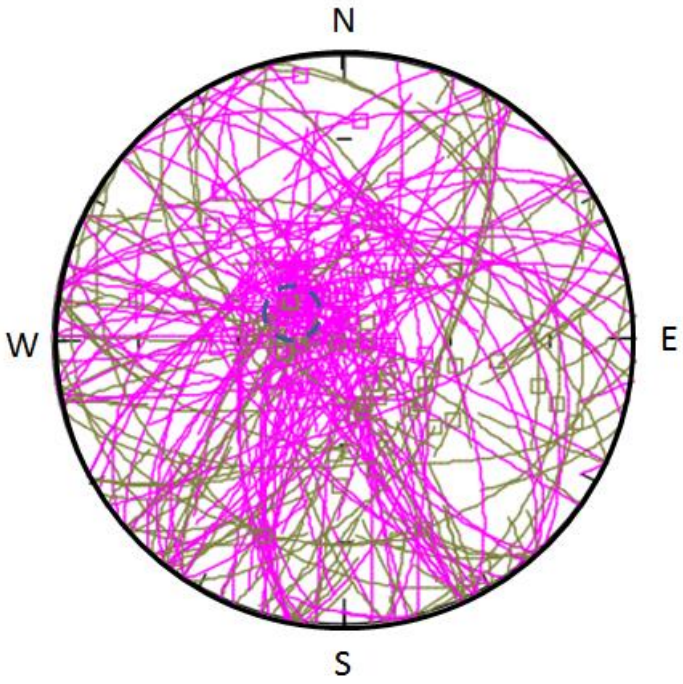

Figure 14. Great circle fits give the mean direction for the $\mathbf{O_H}$ component direction, showing the arcs used for the fits and best point on arc selections. The $\boldsymbol{O_H}$ component exists in samples that lacked a stable end point when they became unblocked. Pink symbols correspond to upper hemisphere directions.

6. Discussion

6.1 Reliability

We successfully decoded 3 components, 2 apparent overprints and 1 presumed characteristic component, and were able to link each to one of the multiple magnetic carriers from our rock magnetic results. The small demagnetization from the liquid nitrogen steps did not reveal a consistent direction, so the MD grains present likely the result of cosmogenic or volcanic dust and the meteorite bombardment observed in the stratigraphic column.

The three components determined at least partially from convergent data, collectively the *P* directions, are the main components of interest. P_W appeared only in highly weathered specimens with a low maximum unblocking temperature and was not distinct from the non-convergent, low-temperature O_L component, so its data were rejected. It is important to note

that even though weak specimens generally have lower unblocking temperatures, blocking temperatures that are too low are potentially too unreliable. In our case, that happened with specimens whose unblocking temperatures were less than half of magnetite, the main magnetic carrier.

We successfully found a magnetozone consistent with formation in the Southern hemisphere in a normal magnetic field in the Uhaku stage (Fig. 15). The normal polarity magnetozone only lasted a short time (consistent with Gallet and Pavlov (1996) and (Pavlov and Gallet, 2005)), so we only uncovered 8 specimens displaying the component, P_N. Though P_N is not well resolved, based on the conodont data in Hints et al. (2012) for the Uuga cliffs near Pakri cape, P_N occurs concurrently with the *Yangtzeplacognathus protoramosus* condont Subzone. The subzone is located near the top of *Pygodus serra* Zone in Figure 1, which also corresponds to the *G. teretiusculus* graptolite Zone (Rasmussen and Stouge, 1989).

Following Vandervoo (1990)'s reliability criteria, we find that P_N passes 5/7 and $P_{R,pre}$ passes 6/7. Field tests were not possible to constrain either pole's age, and P_N lacks sufficient samples, a reliable κ, and α_{95}. The most likely carrier of P is magnetite, but its large variability in maximum unblocking temperature is likely due to the weak NRM values and partial weathering into maghemite. We interpret P_R as syn-sedimentary.

6.2 Agreement with recent work in the area

Our net P_R direction agrees with Plado et al. (2010)'s P_{DD} direction and is consistent with a Southern hemisphere formation in a reversed magnetic field. All statistical comparisons were made using the appropriate reversals test from McFadden and McElhinny (1990). Our $P_{R,K+A}$ direction for the Kunda and Aseri stages agrees with that found in Plado et al. (2016b) for a stratigraphically similar sampling. The statistically significant difference

between this direction and the $P_{R,V\rightarrow LU}$ direction is understandable because apparent polar wander over the duration of the superchron is to be expected, as the Baltica plate was moving (Fig. 6 in Plado et al. (2010)).

The O_L direction is likely the result of weathering of magnetite into maghemite. Plado et al. (2010) noted the presence of a low-coercivity mineral like maghemite affecting the thermal treatment, but did not extract a useful remanence direction. O_L is likely this component. It disappears by $300°C$, is a vector sum of the modern field direction and the paleofield direction, and is in a similar direction to the convergent P_W direction, all consistent with magnetite weathering into maghemite.

The high-temperature component determined from great circle fits, O_H, appears to be carried by hematite, but only minimal amounts of hematite were found in samples from the Uhaku stage. P_N was found only in convergent samples, which agrees with the decreased amount of hematite in the Uhaku stage. Its direction is located within the α_{95} circle for P_N, but P_N only exists as a convergent component, unlike O_H. O_H appears to have a different direction from other directions (with varying ages) in Estonia (e.g. Plado et al. (2010), Plado et al. (2016b), and Preeden et al. (2008)). However, great circle fits can only infer component directions as being somewhere on the arc, so their ability to detect different polarities within the same component, as is the case with a previous observed high-temperature overprint in this area, is limited without lines to provide anchoring. Figure 16 shows that O_H lies on a great circle arc that connects Plado et al. (2010)'s high-temperature S_N and S_R overprints, within their respective α_{95} values. This means that O_H is likely a linear combination of their S_N and S_R, but they were unable to be parsed because O_H lacked any convergent data.

6.3 Ordovician polarity timescale

Our samples start in the *Didymograptus hirundo* Graptolite Zone, which covers the local Volkhov stage (Fig. 1) and corresponds to the upper British Arenig, slightly above the midpoint of the superchron according to Pavlov and Gallet (2005), in the upper part of the Siberian Kimaian stage. Our data agree with Torsvik et al. (1995)'s upper Arenig data but do not show a normal magnetozone in the Llanvrin (in the local Lasnamägi in Figure 15). Instead, our data mirrors Pavlov et al. (2012)'s continuous reverse polarity until the Llandeilo. The stratigraphic position of P_N is comparable to their brief normal magnetozone, followed by another long period of reverse polarity.

Trench et al. (1991), Idnurm et al. (1996), and Opdyke and Channell (1996) proposed composite timescales during the Ordovician that show several reversals during the Darriwillian (Fig. 17). However, we only found a single normal magnetozone, at the upper part of the British Llandeilo. Pavlov et al. (2012) noted that some of the discrepancy between Opdyke and Channell (1996) and the others can be explained by a different biostratigraphic definition for the Cambrian/Ordovician boundary. The small number of samples that we found displaying a normal polarity, synsedimentary component does not support the proposal of a dual-polarity superchron during the Ordovician (Algeo, 1996). Our results agree more closely with Pavlov and Gallet (2005)'s proposed polarity time scale during the Middle Ordovician for the upper half of the superchron.

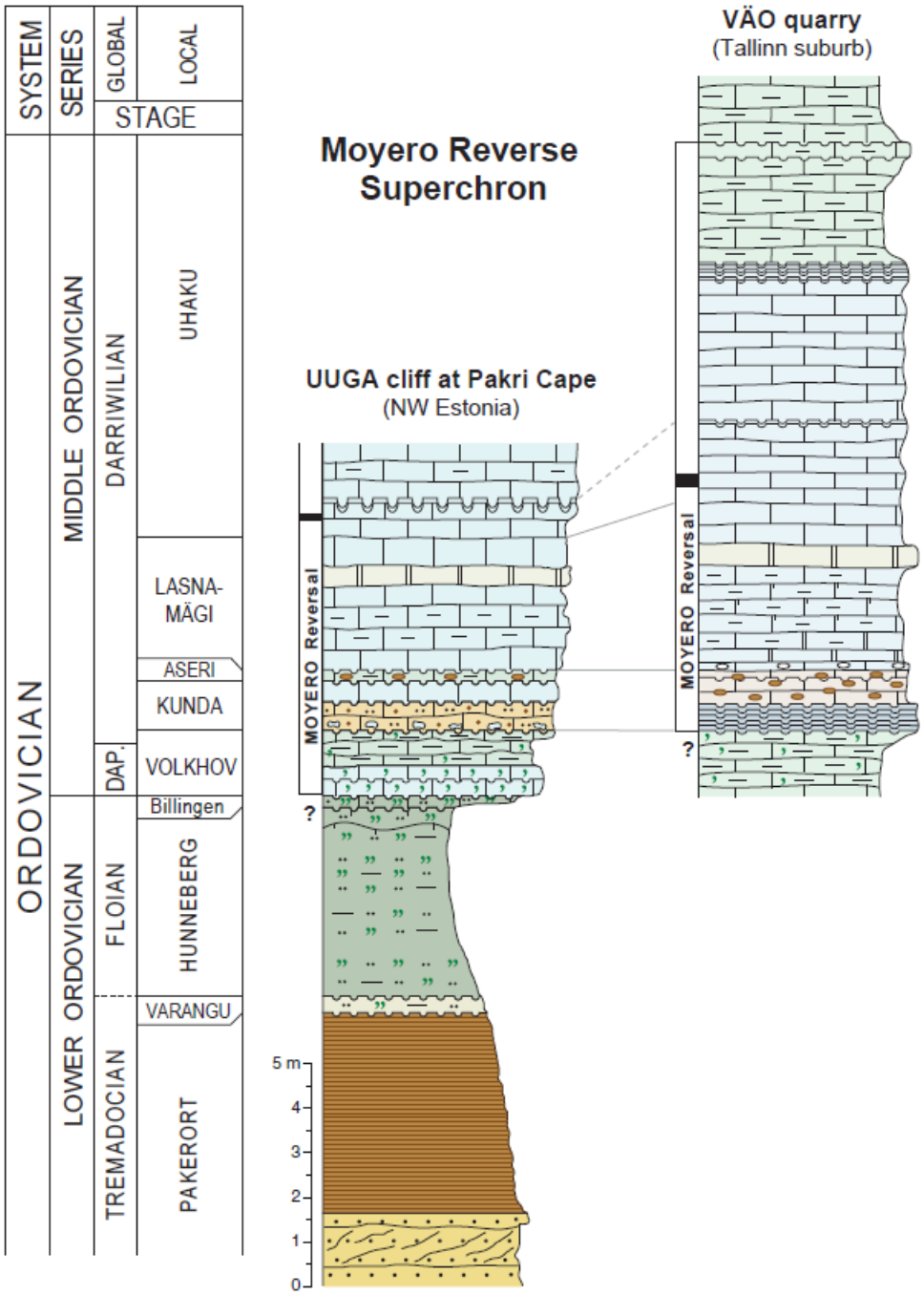

Figure 15. Location of the MRPS in the local, sampled stratigraphy, scaled by stratigraphy. Our samples run from the base of the Volkhov through the end of the superchron into the Uhaku stage. The short normal period is present in two parallel sections and appears to be stratigraphically consistent. The local depositional rate increases with up the stratigraphic column.

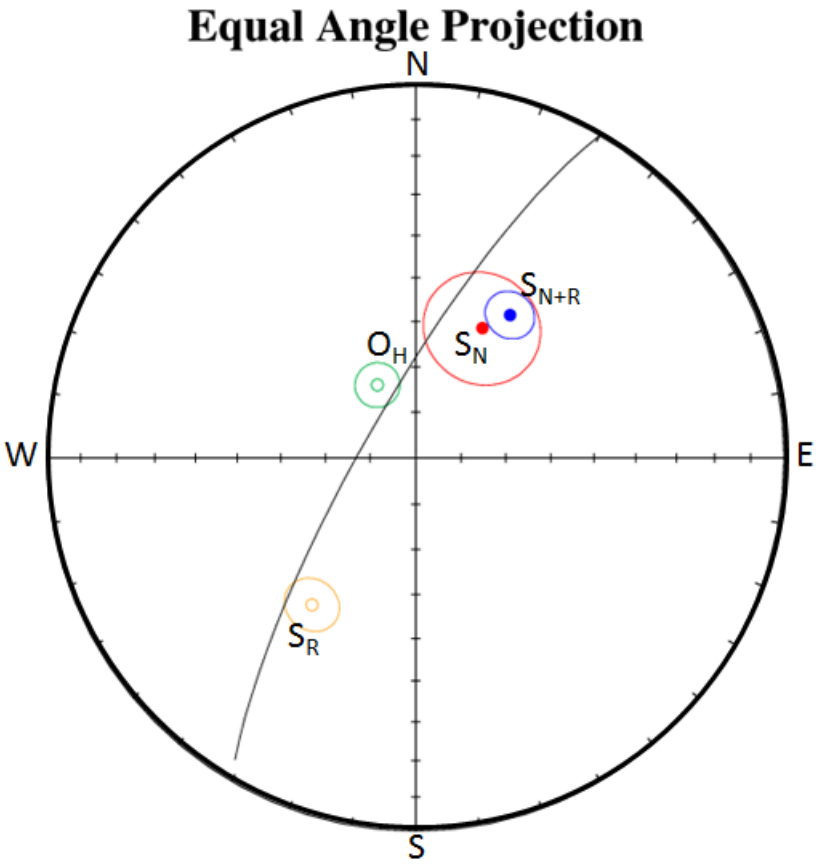

Figure 16. Equal angle projection showing this study's $\boldsymbol{O_H}$ direction compared with Plado et al. (2010)'s $\boldsymbol{S}$ directions. The $\boldsymbol{O_H}$, $\boldsymbol{S_N}$, and $\boldsymbol{S_R}$ directions all plot along the same circle, so $\boldsymbol{O_H}$ is likely a combination of $\boldsymbol{S_N}$ and $\boldsymbol{S_R}$ vectors that were unable to be parsed due to a lack of convergent component data.

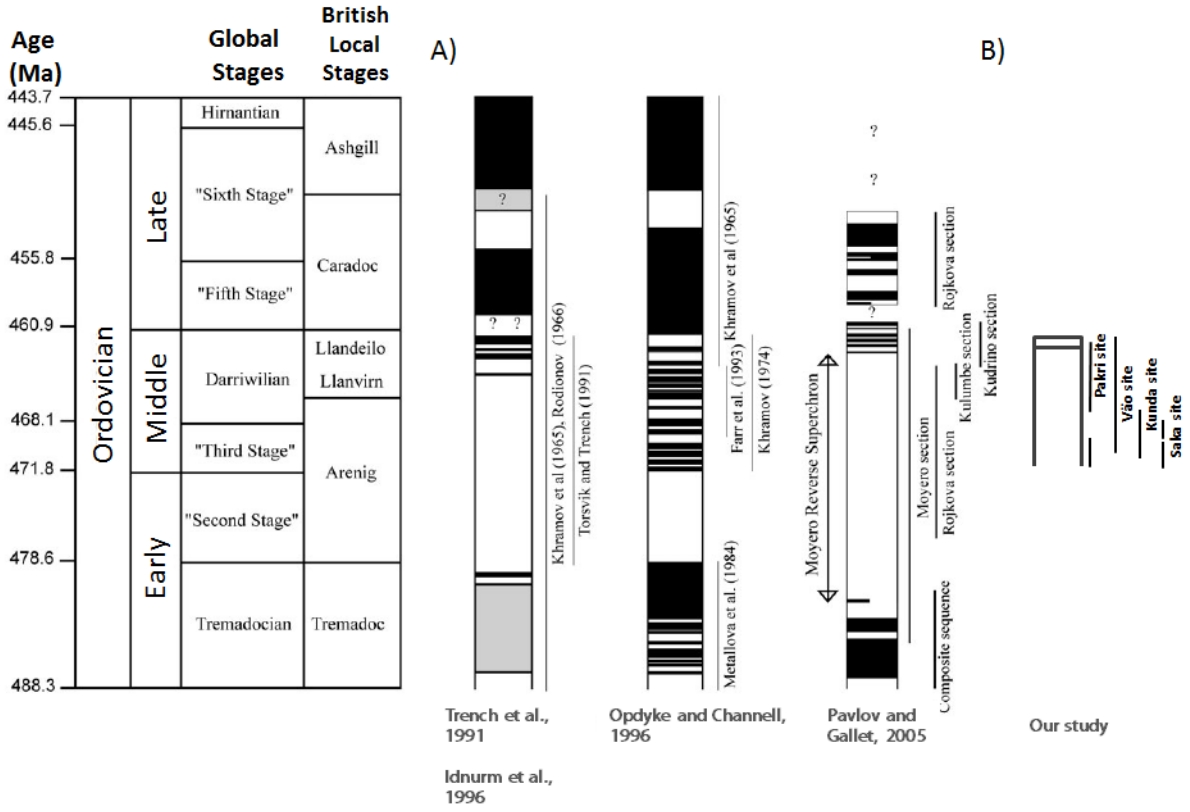

Figure 17. Comparison of Ordovician polarity time scales in order of proposition. A) Adapted from Pavlov and Gallet (2005), with the notes that the timescale discrepancy can be at least somewhat explained by a potentially different biostratigraphic definition for the lower boundary of the Ordovician. B) Our work in Estonia, which agrees with Pavlov and Gallet (2005), put to scale with previous work.

7. Conclusions

The Ordovician specimens from Estonia reported in this study represent the local stratigraphy from the Volkhov to the Uhaku, spanning most of the Middle Ordovician. The specimens taken had exceptionally low NRM values of $5 - 13 \times 10^{-8}\ \frac{Am^2}{kg}$ and low maximum unblocking temperatures, with 84% unblocking by $400°C$. Despite their low magnetizations, useful paleomagnetic data was able to be extracted. The specimens contain primarily single domain, moderately-interacting grains of magnetite, along with smaller amounts of secondary magnetic minerals, hematite and maghemite. We successfully extracted a characteristic direction, which contains a reversal that appears to be stratigraphically consistent across 2 sites and equivalent to previously observed normal

magnetozones that end the MRPS. Many specimens had a low-temperature overprint caused by partial weathering of magnetite into maghe5mite. For highly weathered specimens with weak NRMs like these, additional care must be taken to ensure a convergent component data is still statistically valid. An additional set of specimens had non-convergent medium unblocking temperature components. We used great circle fits to extract a direction for this overprint, which appears to be a linear combination of previously reported overprints. Low maximum unblocking temperatures prevented this component from being well enough resolved to be divided into two polarities. As a result of these data, there now exists a new area, rich in conodonts, that contains both a large portion of and the termination of the MRPS. Dense sampling of the Uhaku local stage will allow precise calibration of the superchron's end.

Acknowledgments

We thank Momoko Shimatsuka, Hiroki Nakahata, Tomoyo Tobita, Valerie Pietrasz and Isaac Hilburn for fieldwork assistance, technical help and support through the project. We would also like to thank and acknowledge the Japan Society for the Promotion of Science (JSPS) KAKENHI (Grant-in-Aid, no. 26257212) for fieldwork expenses, the Summer Undergraduate Research Fellowship program at Caltech to Thomas Chaffee, and named SURF donors, Karen and James Cutts, for providing funding for part of this project.

References

Algeo, T. J., 1996, Geomagnetic polarity bias patterns through the Phanerozoic: Journal of Geophysical Research-Solid Earth, v. 101, no. B2, p. 2785-2814.

Alwmark, C., Schmitz, B., and Kirsimae, K., 2010, The mid-Ordovician Osmussaar breccia in Estonia linked to the disruption of the L-chondrite parent body in the asteroid belt: Geological Society of America Bulletin, v. 122, no. 7-8, p. 1039-1046.

Bauert, H., Einasto, R., and Nõlvak, J., 2014, Stop A5: Väo quarry: 4th Annual Meeting of IGCP 591, v. Field Guide, p. 151-154.

Biggin, A. J., Steinberger, B., Aubert, J., Suttie, N., Holme, R., Torsvik, T. H., van der Meer, D. G., and van Hinsbergen, D. J. J., 2012, Possible links between long-term geomagnetic variations and whole-mantle convection processes: Nature Geoscience, v. 5, no. 8, p. 526-533.

Cisowski, S., 1981, INTERACTING VS NON-INTERACTING SINGLE DOMAIN BEHAVIOR IN NATURAL AND SYNTHETIC SAMPLES: Physics of the Earth and Planetary Interiors, v. 26, no. 1-2, p. 56-62.

Claesson, C., 1978, SWEDISH ORDOVICIAN LIMESTONES - PROBLEMS IN CLARIFYING THEIR DIRECTIONS OF MAGNETIZATIONS: Physics of the Earth and Planetary Interiors, v. 16, no. 1, p. 65-72.

Courtillot, V., and Olson, P., 2007, Mantle plumes link magnetic superchrons to phanerozoic mass depletion events: Earth and Planetary Science Letters, v. 260, no. 3-4, p. 495-504.

Driscoll, P. E., and Evans, D. A. D., 2016, Frequency of Proterozoic geomagnetic superchrons: Earth and Planetary Science Letters, v. 437, p. 9-14.

Enkin, R. J., 2003, The direction-correction tilt test: an all-purpose tilt/fold test for paleomagnetic studies: Earth and Planetary Science Letters, v. 212, no. 1-2, p. 151-166.

Epstein, A. G., Epstein, K. L., and Harris, L. D., 1977, Conodont color alteration - an index to organic metamorphism: Geological Society of America Special Paper, v. 153, p. 108.

Fisher, R., 1953, DISPERSION ON A SPHERE: Proceedings of the Royal Society of London Series a-Mathematical and Physical Sciences, v. 217, no. 1130, p. 295-305.

Fuller, M., Cisowski, S., Hart, M., Haston, R., Schmidtke, E., and Jarrard, R., 1988, NRM: IRM(S) demagnetization plots; An aid to the interpretation of natural remanent magnetization: Geophysical Research Letters, v. 15, no. 5, p. 518-521.

Gallet, Y., and Pavlov, V., 1996, Magnetostratigraphy of the Moyero river section (north-western Siberia): Constraints on geomagnetic reversal frequency during the early Palaeozoic: Geophysical Journal International, v. 125, no. 1, p. 95-105.

Gradstein, F. M., and Ogg, J. G., 2012, Chapter 2 - The Chronostatic Scale, The Geologic Time Scale: Boston, Elsevier, p. 31-42.

Helsley, C. E., and Steiner, M. B., 1969, EVIDENCE FOR LONG INTERVALS OF NORMAL POLARITY DURING CRETACEOUS PERIOD: Earth and Planetary Science Letters, v. 5, no. 5, p. 325-&.

Hints, O., 2014, Stop A1: Pakerort and Uuga Cliffs on the Pakri Peninsula: 4th Annual Meeting of IGCP 591, v. Field Guide, p. 133-137.

Hints, O., Viira, V., and Nõlvak, J., 2012, Darriwilian (Middle Ordovician) conodont biostratigraphy in NW Estonia: Estonian Journal of Earth Sciences, v. 61, no. 4, p. 210-226.

Hounslow, M. W., 2016, Geomagnetic reversal rates following Palaeozoic superchrons have a fast restart mechanism: Nature Communications, v. 7:12507.

Idnurm, M., Klootwijk, H., Theveniaut, H., and Trench, A., 1996, Magnetostratigraphy, *in* Yang, G. C., and Laurie, J., eds., An Australian Phanerozoic Time Scale: Australia, Oxford University Press, p. 22-51.

Irving, E., and Parry, L. G., 1963, THE MAGNETISM OF SOME PERMIAN ROCKS FROM NEW-SOUTH-WALES: Geophysical Journal of the Royal Astronomical Society, v. 7, no. 4, p. 395-411.

Isozaki, Y., Poldvere, A., Bauert, H., Nakahata, H., Aoki, K., Sakata, S., and Hirata, T., 2014, Provenance shift in Cambrian mid-Baltica: detrital zircon chronology of Ediacaran-Cambrian sandstones in Estonia: Estonian Journal of Earth Sciences, v. 63, no. 4, p. 251-256.

Johnson, H. P., Lowrie, W., and Kent, D. V., 1975, STABILITY OF ANHYSTERETIC REMANENT MAGNETIZATION IN FINE AND COARSE MAGNETITE AND MAGHEMITE PARTICLES: Geophysical Journal of the Royal Astronomical Society, v. 41, no. 1, p. 1-10.

Khramov, A. N., and Iosifidi, A. G., 2009, Paleomagnetism of the Lower Ordovician and Cambrian sedimentary rocks in the section of the Narva River right bank: For the construction of the Baltic Kinematic model in the Early Paleozoic: Izvestiya-Physics of the Solid Earth, v. 45, no. 6, p. 465-481.

Kirschvink, J. L., 1980, THE LEAST-SQUARES LINE AND PLANE AND THE ANALYSIS OF PALEOMAGNETIC DATA: Geophysical Journal of the Royal Astronomical Society, v. 62, no. 3, p. 699-718.

Kirschvink, J. L., Isozaki, Y., Shibuya, H., Otofuji, Y., Raub, T. D., Hilburn, I. A., Kasuya, T., Yokoyama, M., and Bonifacie, M., 2015, Challenging the sensitivity limits of Paleomagnetism: Magnetostratigraphy of weakly magnetized Guadalupian-Lopingian (Permian) Limestone from Kyushu, Japan: Palaeogeography Palaeoclimatology Palaeoecology, v. 418, p. 75-89.

Kirschvink, J. L., Kopp, R. E., Raub, T. D., Baumgartner, C. T., and Holt, J. W., 2008, Rapid, precise, and high-sensitivity acquisition of paleomagnetic and rock-magnetic data: Development of a low-noise automatic sample changing system for superconducting rock magnetometers: Geochemistry Geophysics Geosystems, v. 9.

Kobayashi, A., Kirschvink, J. L., Nash, C. Z., Kopp, R. E., Sauer, D. A., Bertani, L. E., Voorhout, W. F., and Taguchi, T., 2006, Experimental observation of magnetosome chain collapse in magnetotactic bacteria: Sedimentological, paleomagnetic, and evolutionary implications: Earth and Planetary Science Letters, v. 245, no. 3-4, p. 538-550.

McFadden, P. L., and McElhinny, M. W., 1988, THE COMBINED ANALYSIS OF REMAGNETIZATION CIRCLES AND DIRECT OBSERVATIONS IN PALEOMAGNETISM: Earth and Planetary Science Letters, v. 87, no. 1-2, p. 161-172.

-, 1990, CLASSIFICATION OF THE REVERSAL TEST IN PALEOMAGNETISM: Geophysical Journal International, v. 103, no. 3, p. 725-729.

McMahon, B. E., and Strangway, D. W., 1968, INVESTIGATION OF KIAMAN MAGNETIC DIVISON IN COLORADO REDBEDS: Geophysical Journal of the Royal Astronomical Society, v. 15, no. 3, p. 265-&.

Meidla, T., 2014, Estonia - a Palaeozoic country: 4th Annual Meeting of IGCP 591, v. Field Guide, p. 111-113.

Meidla, T., Ainsaar, L., and Hints, O., 2014, The Ordovician System in Estonia: 4th Annual Meeting of IGCP 591, v. Field Guide, p. 116-122.

Mertanen, S., 2006, Paleomagnetic and rock magnetic studies from Middle Ordovician limestones in Väo and Pakri, northern Estonia.

Opdyke, N., and Channell, J., 1996, Magnetic stratigraphy: Academic, San Diego.
Pavlov, V., and Gallet, Y., 1998, Upper Cambrian to Middle Ordovician magnetostratigraphy from the Kulumbe river section (northwestern Siberia): Physics of the Earth and Planetary Interiors, v. 108, no. 1, p. 49-59.
-, 2005, A third superchron during the Early Paleozoic: Episodes, v. 28, no. 2, p. 78-84.
Pavlov, V. E., Veselovskiy, R. V., Shatsillo, A. V., and Gallet, Y., 2012, Magnetostratigraphy of the Ordovician Angara/Rozhkova River section: Further evidence for the Moyero reversed superchron: Izvestiya-Physics of the Solid Earth, v. 48, no. 4, p. 297-305.
Peters, C., and Dekkers, M. J., 2003, Selected room temperature magnetic parameters as a function of mineralogy, concentration and grain size: Physics and Chemistry of the Earth, v. 28, no. 16-19, p. 659-667.
Plado, J., Ainsaar, L., Dmitrijeva, M., Põldsaar, K., Ots, S., Pesonen, L. J., and Preeden, U., 2016a, Magnetic susceptibility of Middle Ordovician sedimentary rocks, Pakri Peninsula, NW Estonia: Estonian Journal of Earth Sciences, v. 65, no. 3, p. 125-137.
Plado, J., Preeden, U., Joeleht, A., Pesonen, L. J., and Mertanen, S., 2016b, Palaeomagnetism of Middle Ordovician Carbonate Sequence, Vaivara Sinimaed Area, Northeast Estonia, Baltica: Acta Geophysica, v. 64, no. 5, p. 1391-1411.
Plado, J., Preeden, U., Pesonen, L. J., Mertanen, S., and Puura, V., 2010, Magnetic history of Early and Middle Ordovician sedimentary sequence, northern Estonia: Geophysical Journal International, v. 180, no. 1, p. 147-157.
Poldvere, A., Isozaki, Y., Bauert, H., Kirs, J., Aoki, K., Sakata, S., and Hirata, T., 2014, Detrital zircon ages of Cambrian and Devonian sandstones from Estonia, central Baltica: a possible link to Avalonia during the Late Neoproterozoic: Gff, v. 136, no. 1, p. 214-217.
Preeden, U., 2009, Remagnetizations in sedimentary rocks of Estonia and shear and fault zone rocks of southern Finland [Doctor of Philosophy: University of Tartu, 52 p.
Preeden, U., Mertanen, S., Elminen, T., and Plado, J., 2009, Secondary magnetizations in shear and fault zones in southern Finland: Tectonophysics, v. 479, no. 3-4, p. 203-213.
Preeden, U., Plado, J., Mertanen, S., and Puura, V., 2008, Multiply remagnetized Silurian carbonate sequence in Estonia: Estonian Journal of Earth Sciences, v. 57, no. 3, p. 170-180.
Rasmussen, J. A., and Stouge, S., 1989, MIDDLE ORDOVICIAN CONODONTS FROM ALLOCHTHONOUS LIMESTONES AT HOYBERGET, SOUTHEASTERN NORWEGIAN CALEDONIDES: Norsk Geologisk Tidsskrift, v. 69, no. 2, p. 103-110.
Smethurst, M. A., Khramov, A. N., and Pisarevsky, S., 1998, Palaeomagnetism of the Lower Ordovician Orthoceras Limestone, St. Petersburg, and a revised drift history for Baltica in the early Palaeozoic: Geophysical Journal International, v. 133, no. 1, p. 44-56.
Torsvik, T. H., Tait, J., Moralev, V. M., McKerrow, W. S., Sturt, B. A., and Roberts, D., 1995, ORDOVICIAN PALEOGEOGRAPHY OF SIBERIA AND ADJACENT CONTINENTS: Journal of the Geological Society, v. 152, p. 279-287.
Trench, A., McKerrow, W. S., and Torsvik, T. H., 1991, ORDOVICIAN MAGNETOSTRATIGRAPHY - A CORRELATION OF GLOBAL DATA: Journal of the Geological Society, v. 148, p. 949-957.
Vandervoo, R., 1990, THE RELIABILITY OF PALEOMAGNETIC DATA: Tectonophysics, v. 184, no. 1, p. 1-9.

Ward, P. D., Hurtado, J. M., Kirschvink, J. L., and Verosub, K. L., 1997, Measurements of the Cretaceous paleolatitude of Vancouver Island: Consistent with the Baja British Columbia hypothesis: Science, v. 277, no. 5332, p. 1642-1645.

Highlights

- The Moyero Superchron is studied in Estonia, detecting a short normal period that ends it
- A high-sensitivity RAPID system was successfully used on weakly magnetized sediments
- The paleopole, a high-temperature overprint, and the location of the end of the superchron were found to be similar to previous work
- Rockmagnetics of the sites are reported and indicate multiple magnetic carriers